Designing high sensitivity surface plasmon resonance sensor using a left-handed material layer

A. Bezza, A. Cherifi and B. Bouhafs

University of Tlemcen, Faculty of Sciences, Theoretical Physics Laboratory, Tlemcen, 13000. Algeria.
e-mail: cherifi_physics@yahoo.com

Received 3 May 2022; accepted 24 August 2022

In this contribution, we propose a new plasmonic configuration that can be functionalized in two wavelength regimes to generate a single interface mode or multiple interface modes. The structure comprises a negative metamaterial or Left-Handed Material (LHM) coated on 2S2G-glass prism and adjacent with a sensing medium. According to the results, the negative metamaterial thickness affects significantly the potential of the structure to operate as conventional plasmonic structured formed by Fabry-Perot cavities. Additionally, we, also show that the structure can be used as a plasmonic refractive index sensor defined in the range of 1 to 1.53 refractive index unit (RIU) where the full width at half maximum (FWHM) of the SPR curve on the characteristic's manipulation such that FWHM of p-reflectivity decreases for thick LHM layer. To understand the obtained results, the optical response from the proposed waveguide was numerically predicted by the use of the transfer matrix method (TMM) and Fresnel's theory. In addition, the potentials of the designed waveguide as an optical modulator and Fabry-Perot interferometer are also presented.

Keywords: Plasmonic configuration; negative metamaterial; Fabry-Perot cavity; transfer matrix method; angular analysis.

DOI: https://doi.org/10.31349/RevMexFis.69.021002

1. Introduction

The past decade has witnessed growing interest in investigating the propagation properties of resonant phenomena for their ability to confine photons at the nanoscale regime. Such phenomena when stimulated with cohent light, are correlated to electric fields of evanescent charater in both media of an interface while it is probed in the attenuated total reflection (ATR) technique. Generally, the detection methods for analyzing resonant phenomena that sustain optical devices include angle interrogation, wavelength interrogation and phase interrogation. In the case of wavelength interrogation, polychromatic light is required as the incident light. However, for angle interrogation, only monochromatic light is required, it is possible to achieve higher signal-to-noise ratio due to the wavelength and power light stability of the operating source. Thus, angle interrogation is adopted in this work. Additionally, the fundamental characteristic known to SPR is their high sensitivity to small fluctuations in refractive index (RI) of a testing medium taken in contact with a metallic surface of abundant free electrons.Resonant phenomena refer to surface plasmon polaritons (SPR) excitation and have been investigated in several approaches, principally based on altering metallic thin films and dielectrics of opposite dielectric permittivity's. Otherwise, SPR can be supported in appropriate conditions in terms of polarization of an incident light beam, and optical properties of active materials like noble metals (silver, gold, aluminum, semiconductor, metamaterials, etc.) enclosed between a substrate and sensing medium. In the case of Kretschman configuration [1] performed between a substrat of RI, n_p and an active metal (permittivity, $\epsilon_m = \epsilon^{'} + i\epsilon^{''}$ with $|\epsilon^{''}| << \epsilon^{''}$) in contact with a dielectric (RI, n_S), SPR occurs at an incidence angle, θ_{SPR} that can be predicted from the behavior of reflectance/transmittance behaviors. The above optical responses from the configuration evolved are based on Fresnel 'theory and boundary conditions that fulfil the propagating electric fields on the interfaces within different media of the device. These basic electromagnetic calculations can be found in details elsewhere [2,3].

Due to the absorption mechanism, SPs excitation is pronounced by a minimum in the reflectance light. However, the later optical response plays a significant interest to characterize the performance of the designed plasmonic configuration in terms of the limits of its sensitivity that depends essentially on the optical properties of the active metallic surface and sensing medium.

As an alternative system for the sensor miniaturization, here we propose a concept of an SPR sensor based on a chalcogenide (2S2G) glass-prism as an optical coupler. Nevertheless, chalcogenide glass showed a relatively high sensitivity and good abilities for sensing large refractive index of aqueous solution closest to that of water. In our study, we analyze the conditions of an SPR excitation on the impacted parameters of the structure and examine the sensing characteristics of the system in Kretschmann approach consisting of four layered media.

2. The conventional configuration and basic theory

2.1. Fabry-Perot interferometers based SPR sensors (FPIs-SPR)

2.1.1. *Fabry-Perot interferometers*

For decades, Fabry-Perot interferometers (FPIs) based SPR sensors have been employed in chemical sensing, biosensing, gas sensing, ultrasonic sensing, optical communication, optical modulation, nanofluidic dynamics analysis, and spectrum endoscope optical imaging. When light shines through a cavity enclosed by two reflective parallel surfaces, the Fabry-Perot interferometer harnesses the phenomena of multiple beam interference. When light strikes one of the surfaces, a portion of it is transmitted, while the remainder is reflected back. The end result is that a single beam is split into numerous beams that interfere with one anotherThe reflected beams will interfere constructively if he increased optical path length of the reflected beam (due to multiple reflections) is an integral multiple of the light's wavelength. The interference maximum sharpens as the number of reflections inside the cavity increases. Finesse and free spectral range can be understood using the Fabry-Perot interferometer as a spectroscopic tool [4].

As seen in the Fig. 1, when a thin layer of d thickness with semi-reflective walls is illuminated of a monochromatic plane wave represented by E^i the electric field and characteristic by λ wavelength, the rays emerging from the layer are out of phase with one another because some have, by bouncing within, fallen behind the others.

According to the Snell-Descartes law $\sin\theta_i = n_1 \sin\theta_1$, incident light is refracted at an angle θ_1 if it arrives at an angle θ_i, where is the thin layer's refractive index. Propagation that is ongoing at interfaces. Reflectivity and transmission concepts. The wave vectors of the partial waves are shown by the arrows. The variables next to the arrows show the phases of the related electric field's values. Equations (1a) and (1b)

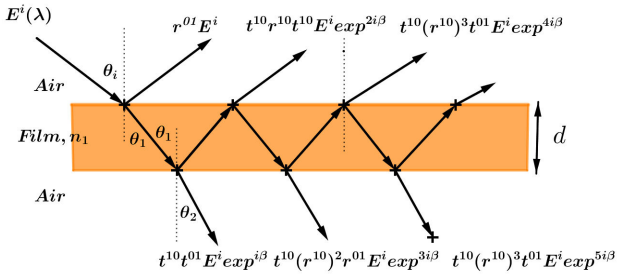

FIGURE 1. Schematic representation of a Fabry-Perot interferometer showing how light rays are partially reflected inside the cavity before exiting.

defining the Fresnel coefficients (reflection r and transmission t at the interface) d are given by:

$$r^{01} = \frac{n_1 k_{z0} - k_{z1}}{n_1 k_{z0} + k_{z1}}, \tag{1a}$$

$$t^{01} = \frac{1}{n_1}(1 + r^{01}), \tag{1b}$$

where $k_{z0} = (2\pi/\lambda)\cos\theta_i$, $k_{z1} = (n_1^2 - \sin^2\theta_i)^{0.5}$ $r^{01} = -r^{10}$, $t^{01}t^{10} = (1 + r^{01})(1 + r^{10})$ and $\beta = d.k_{z1}$.

2.1.2. *Condition of excitation of the SPR*

Advances in electromagnetic theory have helped explain these anomalies by the excitation of surface electromagnetic resonance, called plasmon resonance. They are excited using different types of coupling devices presented in Fig. 2:

1. Prism coupling, which is based on total internal reflection to transmit to the interface an evanescent wave whose parallel wave vector is increased by the refraction index of the prism.

2. Network coupling (periodic roughness), which transfers the vector of the reciprocal network to the incident parallel wave vector.

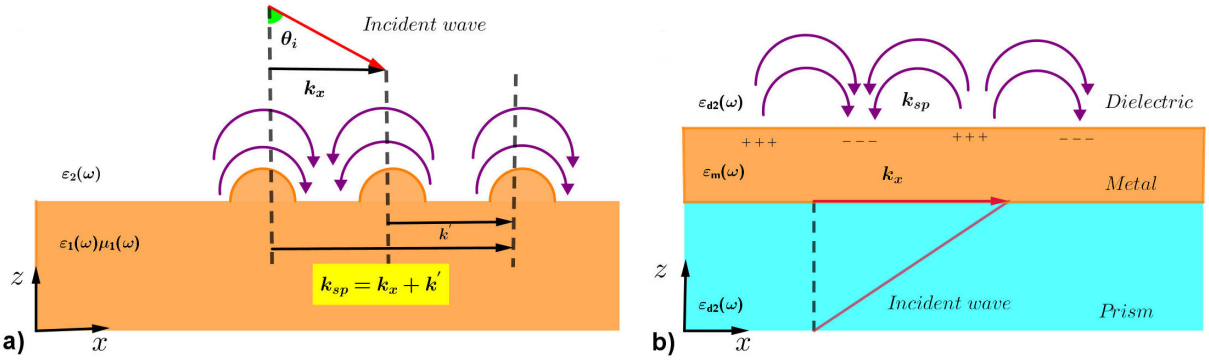

FIGURE 2. Schematic representation of the Attenuated Total Reflection (ATR) device allowing excitation of the surface plasmon by an incident wave of TM polarization and wavelength and the relationship between the tangential component of the excitation wave vector and the wave vector of surface plasmons K_{SP} for: a) Kretschmann configuration, b) A diffraction grating.

The incidence medium is an optical prism, RI n_p whose interest is to match the component according to z of the wave vector, $k_x = (n_p/c)\sin\theta_i$ to that of the SP, k_x likely to be excited under conditions, $\theta_i > \theta_C$ (critical angle). Considere the active metal is a thin layer of thickness d, the characteristics (minimum intensity, angular position, confinement and width at half height) of the plasmon response are manipulated on the intensity of the beam from reflection to l prism/metal interface (Cf. Fig. la)). Under the influence of structure parameters, the Surface Plasmons (SPs) are generated by an external light excitation of polarization TM under an angle of incidence, θ_i on which the reflected intensity depends.According to Maxwell's equations: ($\nabla \times H = -\partial D/\partial t = 0$, and $\nabla \times E = -\partial B/\partial t$), in the case of a planar interface the wave propagation equation can be deduced from the usual equation:

$$\nabla^2 E - \frac{\epsilon_r}{C}\frac{\partial E}{\partial t} = 0. \quad (2)$$

Here, ϵ_r is the dielectric constant associated with the electron motion and C the speed of light in vacuum, respectively. In the optical process of SP excitation, a portion of the incident energy is transferred by the absorption mechanism to the SP that dissipate thereafter through the metallic film. Thus, the result is a drop in reflected intensity which is marked by the presence of a minimum over the resonance angle. However, the angular localization noted, θ_{SPR} is highly sensitive to any fluctuation of the RI of the dielectric medium which induces an angular shift noted, θ_{SPR}. This last property means that the performance of any nano-metric structure for the chemical biodetection of substances is based on the observation of the angular offset at small variations in the index of the analysis medium.

2.2. SPR characteristics based Metamaterials

2.2.1. Metamaterials

The name "metamaterial" was initiated by Rodger M. Walser [4] to attribute it to a macroscopic composite. Nowadays, the term metamaterial refers to a class of microscopic and macroscopic engineering material. There are several types of MMs, which are classified according to the signs of their dielectric permittivity and permeability (see Fig. 3). In addition, photonic crystals are also considered as metamaterials [5]. Several experimental works have been studied by groups [6-7] to confirm the existence of the negative refractive index property for a metamaterial. In 1968, V. Veselago [8] advanced, theoretically, and for the first time the concept of metamaterial having simultaneously negative real parts of the permittivity electric and magnetic permeability. The terminology assigned to this class of metamaterial is "left hand material (LHM for short)"; and we also say negative index metamaterial (NIM), the dielectric permittivity ϵ and the magnetic permeability μ. The fundamental quantities often used to characterize a medium on the response of the electromagnetic fields of a wave are the permittivity and the permeability

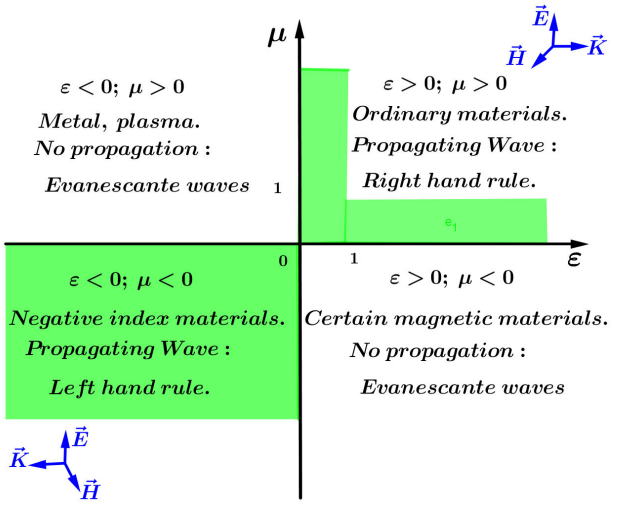

FIGURE 3. Conventional classes of metamaterials characterized on the parameters of (ϵ, μ) [9].

(ϵ, μ). In the four dials (I, II, III, and IV) of the orthogonal coordinate system. To give a complement to this part, we report on Fig. 2 the different types of metamaterials conventionally defined according to the signs of (ϵ, μ).

The work undertaken analytically that we will describe in this chapter is limited to the case of a metamaterial of the LHM type whose permittivity and permeability are experimental values tabulated according to the reference [10].

2.2.2. Propagation conditions in a metamaterials

Let us considere the configuration displayed in Fig. 4, formed by an interface between medium 1 in which an incident wave propagates under the angle θ_i in a material medium i, of wave vector, k_i taken in contact with a medium 2. Thus, the incident wave will partialy reflected (wave vector k_r) and refracted (of wave vector k_t). For such propagation condition, it should be noted that Snell's law follows the form:

$$n_1 \sin\theta_i = n_2 \sin\theta_t. \quad (3)$$

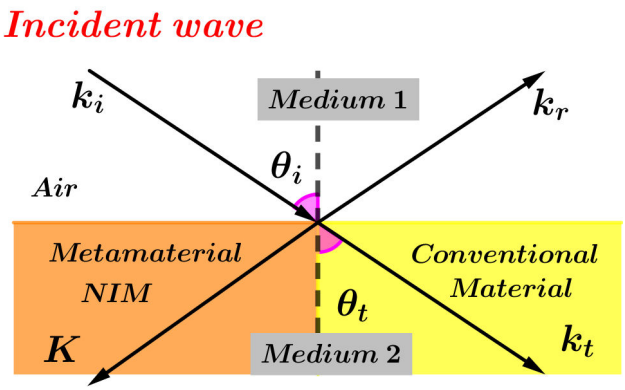

FIGURE 4. Propagation of a plane light wave near an interface limited by two material media, where NIM is the acronym for: Material with Negative Refractive Index.

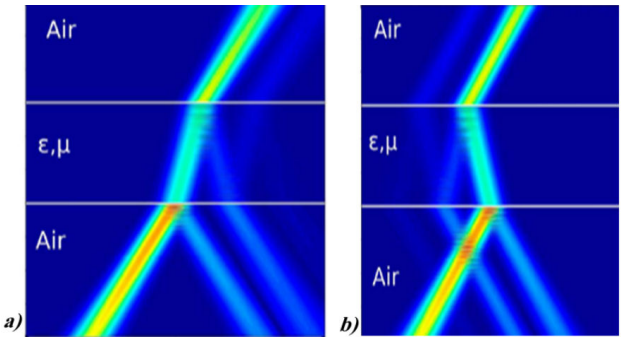

FIGURE 5. Light beam propagation through a metamaterial for two properties, for: a) ϵ and μ simultaneously positive and for b) ϵ and μ simultaneously negative.

Considering that the medium 2 is a conventional material, the refracted wave is described by the wave vector k_r deviated by an angle θ_t to the right of the normal direction zz'. On the other hand, in the case where the medium 2 is a metamaterial type (NIM), the refraction in this medium is produced to the left of the normal zz' ; that is to say a refraction which is opposite to the usual refraction In the two cases of material (1 or 2), Snel's law always remains valid:

1. The medium of incidence is considered the ambient air, index n_1.
2. The transmission medium is a metamaterial or a conventional material, RI n_2.

Such a propagation property produced on an interface in the presence of a metamaterial has been observed experimentally by the group of Ref. [5]. Let us consider a plane wave propagating in a metamaterial (LHM) and which is described by the electric and magnetic fields according to the forms:

$$E = \mathrm{Re}\left\{E \exp\left(i\left[K.r - \omega t\right]\right)\right\}, \tag{4a}$$

$$H = \mathrm{Re}\left\{H \exp\left(i\left[K.r - \omega t\right]\right)\right\}, \tag{4b}$$

In each medium subscribed by, j the electromagnetic fields (E, H) are expressed as we deduce the vector expressions of E and H:

$$k \times E_j = i\mu \frac{\omega}{C} H_j, \tag{5a}$$

$$k \times H_j = -i\epsilon \frac{\omega}{C} E_j, \tag{5b}$$

where k represents the wave vector given as:

$$k^2 = \frac{\omega}{C}^2 \epsilon\mu. \tag{5c}$$

According to the forms of the Eq. (5a), the trihedra (E,H,k) characterizes a material with left hand (LHM) when the quantities and are simultaneously negative and where the trihedron is inverted.

By considering an electric field of polarization (TM), the Poynting vector is written:

$$\langle S \rangle = \frac{1}{2}\mathrm{Re}\left(E \times H\right) = \frac{C}{2\mu\omega} p\left(E \times p\right) = \frac{Ck}{2\mu\omega}. \tag{6}$$

In addition, from this calculation, we conclude that for $\mu < 0$, the wave vector k (see Eq. (5c)) has an opposite direction to that of the Poynting vector (p). Such a conclusion is also analogous for the condition of an electric field of polarization (TE) when $\epsilon < 0$. Thus, the control of the propagation of a plane wave in a metamaterial is recorded by a phase speed of the wave which is always in the opposite direction to the flow of electromagnetic energy.

In addition, it is obvious that from the refractive index of the metamaterial:

$$n^2\left(\omega\right) = \epsilon(\omega)\mu(\omega). \tag{7}$$

For ϵ and μ simultaneously negative, the refractive index is also negative. Theoretical considerations on losses have not been discussed in this chapter. It is basically known that an electromagnetic wave is systematically attenuated by propagating in a given material. This optical effect is implied by the complex terms of the optical properties (μ, ϵ).

2.2.3. Optical functionalization parameters

In the hypothesis of including losses due to the absorption of a wave propagating in a material, it is advisable to adopt models on the electromagnetic quantities; *i.e.*, electric permittivity and magnetic permeability defined, respectively as follows [12]:

$$\epsilon_{NIM}(\omega) = 1 - \frac{\omega_{p,e}^2}{\omega^2 - \omega_{0,e}^2 + i\gamma_e\omega} = \epsilon^{'} + i\epsilon^{''}, \tag{8a}$$

$$\mu_{NIM}(\omega) = 1 - \frac{\omega_{p,m}^2}{\omega^2 - \omega_{0,m}^2 + i\gamma_m\omega} = \mu^{'} + i\mu^{''}, \tag{8b}$$

With $\omega_{p,e}, \gamma_e, \omega_{0,e}$ which designate the plasma frequency, relaxation term and resonance frequency respectively due to the contribution of the electric field of the wave. Similarly, $\omega_{p,m}, \gamma_m, \omega_{0,m}$ denote the plasma frequency, relaxation term and resonance frequency respectively due to the contribution of the magnetic field of the wave.

2.3. Design consideration and analytical resolution

We will now see the case of the existence of N layers stacked and excited by an electromagnetic wave [13]. For the calculation of the reflectivity R_p of a plane polarized wave p on a medium made up of N isotropic layers and dielectric constants ϵ_k, we used the matrix formalism well adapted with the Matlab software. This formalism, based on the calculation of Fresnel coefficients, which takes into account the metallic or Metamaterial layers with dielectric layers.

This involves expressing the electric E_k and magnetic fields H_k across the N layers of the geometry (see Fig. 6), taking into account a matrix at each interface $(k-1)/k$ and a propagation matrix in each layer k. We considered a stratified

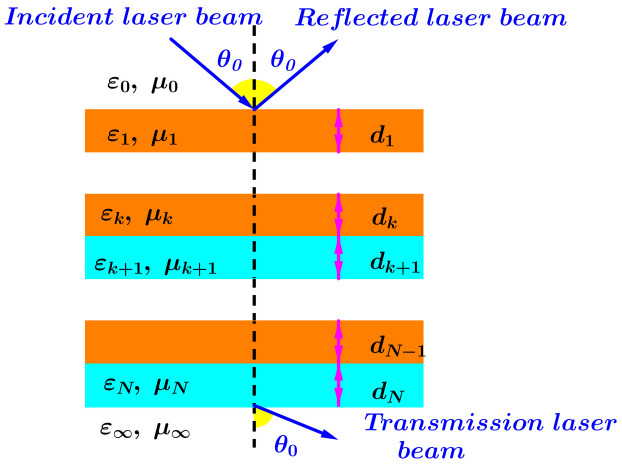

FIGURE 6. Propagation of plane waves in a multilayer film system; The arrows represent the wave vectors of the forward and backward propagation waves.

layer of thickness d (medium 1) between two homogeneous half space:

$$E_0 = E_0^+ \begin{pmatrix} 0 \\ 0 \\ \frac{-k_x}{k_{0,z}} \end{pmatrix} \exp(ik_{0,z}z) + E_0^- \begin{pmatrix} 0 \\ 0 \\ \frac{k_x}{k_{0,z}} \end{pmatrix} \exp(-ik_{0,z}z),$$

$$E_1 = E_1^+ \begin{pmatrix} 0 \\ 0 \\ \frac{-k_x}{k_{1,z}} \end{pmatrix} \exp(ik_{1,z}(z-d)) + E_1^- \begin{pmatrix} 0 \\ 0 \\ \frac{k_x}{k_{1,z}} \end{pmatrix} \exp(-ik_{1,z}(z-d)),$$

$$E_2 = E_2^+ \begin{pmatrix} 0 \\ 0 \\ \frac{-k_x}{k_{2,z}} \end{pmatrix} \exp(ik_{2,z}z). \quad (9)$$

Where the components k_x and k_{zp} of the incident wavevector, k are given by equations:

$$k_x = \frac{2\pi}{\lambda} n_p \sin\theta_i, \quad (10a)$$

$$k_{z0} = \frac{2\pi}{\lambda} n_p \cos\theta_i, \quad (10b)$$

$$k_{zj} = (\epsilon_j \mu_j - \epsilon_p \sin^2\theta_i)^{1/2}. \quad (10c)$$

These set of equations stands wave vector components along z direction in each layer indexed, j with, $j = 1$ and 2 respectively. Exploiting the continuity of yield after straightforward manipulation as:

$$\begin{pmatrix} E_0^+ \\ E_0^- \end{pmatrix} = \frac{1}{2} \begin{pmatrix} 1+q_1\beta_1 & 1-q_1\beta_1 \\ 1-q_1\beta_1 & 1+q_1\beta_1 \end{pmatrix} \times \begin{pmatrix} 1 & 0 \\ 0 & \exp(ik_{z1}z) \end{pmatrix} \begin{pmatrix} E_1^+ \\ E_1^- \end{pmatrix}, \quad (11a)$$

$$\begin{pmatrix} E_1^+ \\ E_1^- \end{pmatrix} = \begin{pmatrix} \exp(-ik_{z1}z) & 0 \\ 0 & 1 \end{pmatrix} \cdot \frac{1}{2} \times \begin{pmatrix} 1+q_2\beta_2 & 1-q_2\beta_2 \\ 1-q_2\beta_2 & 1+q_2\beta_2 \end{pmatrix} \begin{pmatrix} E_2^+ \\ 0 \end{pmatrix}, \quad (11b)$$

where $q_k = k_{zj}/k_{(z,j+1)}$ and $\beta_k = \epsilon_{(j+1)}/\epsilon_j$. Equations (10a) and (10b) can be combined to give:

$$\begin{pmatrix} E_0^+ \\ E_0^- \end{pmatrix} = T_{01}.\phi_1.T_{02} \begin{pmatrix} E_2^+ \\ 0 \end{pmatrix}, \quad (12a)$$

$$T_{01} = \frac{1}{2} \begin{pmatrix} 1+q_1\beta_1 & 1-q_1\beta_1 \\ 1-q_1\beta_1 & 1+q_1\beta_1 \end{pmatrix}, \quad (12b)$$

$$T_{02} = \begin{pmatrix} 1+q_2\beta_2 & 1-q_2\beta_2 \\ 1-q_2\beta_2 & 1+q_2\beta_2 \end{pmatrix}, \quad (12c)$$

and

$$\phi_1 = \begin{pmatrix} \exp(-ik_{z1}z) & 0 \\ 0 & \exp(ik_{z1}z) \end{pmatrix}. \quad (12d)$$

From these formulas, we can deduce a general relationship for writing matrix M, as this matrix $[M]$ is the product of many matrices where there are layers:

$$\begin{pmatrix} E_0^+ \\ E_0^- \end{pmatrix} = M \begin{pmatrix} E_{n+1}^+ \\ 0 \end{pmatrix}, \quad (13a)$$

with

$$M = T_{01}.\phi_1.T_{02}.....T_{n,n+1} \quad (13b)$$

Finaly, TM-reflectivity from the multilayer is then given for each pulse or wavelength whose shape is linked by the elements of matrix M according to the following relationships:

$$R(\omega, k_x) = \frac{|E_0^-|^2}{|E_0^+|^2} = \frac{|M_{12}|}{|M_{22}|^2}. \quad (14)$$

From which $E_{(n+1)}^+$ cancels out.

3. SPR characteristics under Krestchmann configuration based on LHM monolayer

3.1. Effect of LHM layer thickness

The structure illustrated in Fig. 7a) is assumed to be irradiated with an incident light beam of 1 μm -wavelength. Due this monochromatic beam, electromagnetic properties of the active LHM layer of thickness, d are described by the electric permittivity, $\epsilon(\lambda) = -4 + i0.001$ and magnetic permeability, $\mu(\lambda) = -2.4 + i0.001$ [14]. The LHM is coated on the base of a glass prism (2S2G) of refractive index, $n_p(\lambda) = 2.31$ [15]. The outer medium assumed to be the

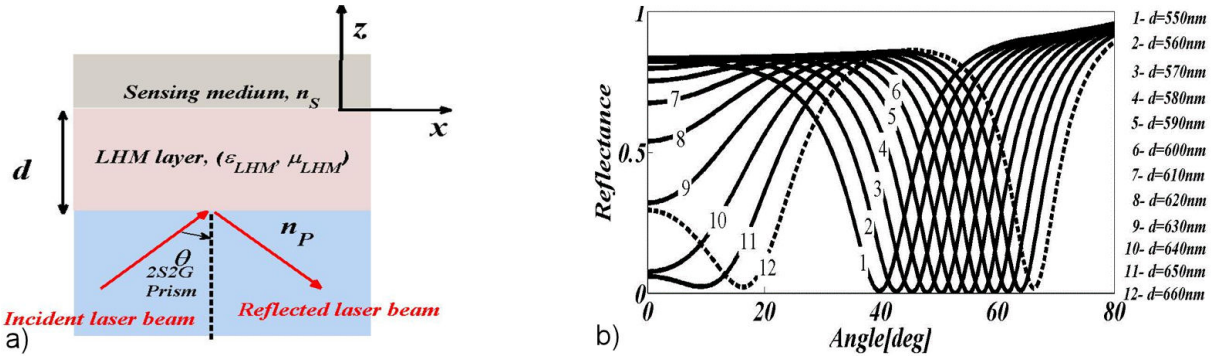

FIGURE 7. a) Kretschmann configuration based on LHM layer enclosed between (2S2G) glass prism of a high index and sensing medium (water, $RI = 1.33$). b) Reflectance curves for different thicknesses of LHM layer. The refractive indices used are: $n_P = 2.31$, $\epsilon_{LHM} = -4 + 0.001i$, $\mu_{LHM} = -2.4 + 0.001i$; $n_{LHM} = -(\epsilon_{LHM} \times \mu_{LHM})^{0.5}$ and $n_S = 1.33$.

TABLE I. Specific SPR features calculated on p-reflectivity spectra of the proposed LHM layer sensor at 1000 nm-wavelength.

d, nm	550	560	570	580	590	600	610	620	630	640	650	660
R(%)	0.86	0.65	0.47	0.26	0.13	0.035	0.019	0.035	0.23	0.63	1	1.87
θ_{spr}	39.87	42.55	45.22	47.59	50.3	52.71	55.12	57.26	59.43	61.94	63.95	66.35
$\triangle\theta_{0.5}$	13.97	13.11	12.53	12.01	11.58	11.2	10.8	10.41	10.12	10.01	9.57	9.52

sensing medium is water of refractive index, $n_s = 1.33$. Using above data, p-reflectance curves are reported in Fig. 7a), for different LHM thicknesses, d. The optimization of LHM layer thickness reveals the determinate point in deciding the performance of the proposed SP sensor. It can be observed that LHM layers thickness:

- Shifts the resonance condition from lower incident angle, 39.97° to higher incident angle, 66.35°.
- Narrows the full width at half maximum (FWHM) from 13.97° to 9.52°.
- Increases the dip depth of reflectance. SP resonance peak features are listed in Table I.

From p-reflectance plots with respect to LHM thickness, resonance condition, dip depth, and FWHM related to the SP mode exhibited from the designed sensor can be derived as reported in the inset of Fig. 8. The acceptable conditions in terms of minimum dip depth, and reduced FWHM are achieved for 610 nm LHM thickness. As reported in Table I, quality factor of the designed sensor can be evaluated as:

$$Q = \frac{\theta_{SPR}}{\triangle\theta_{0.5}} = \frac{55.12}{10.8} = 5.1. \tag{15}$$

From p-reflectance plots with respect to LHM thickness, resonance condition, dip depth, and FWHM related to the SP mode exhibited from the designed sensor, depends indirectly

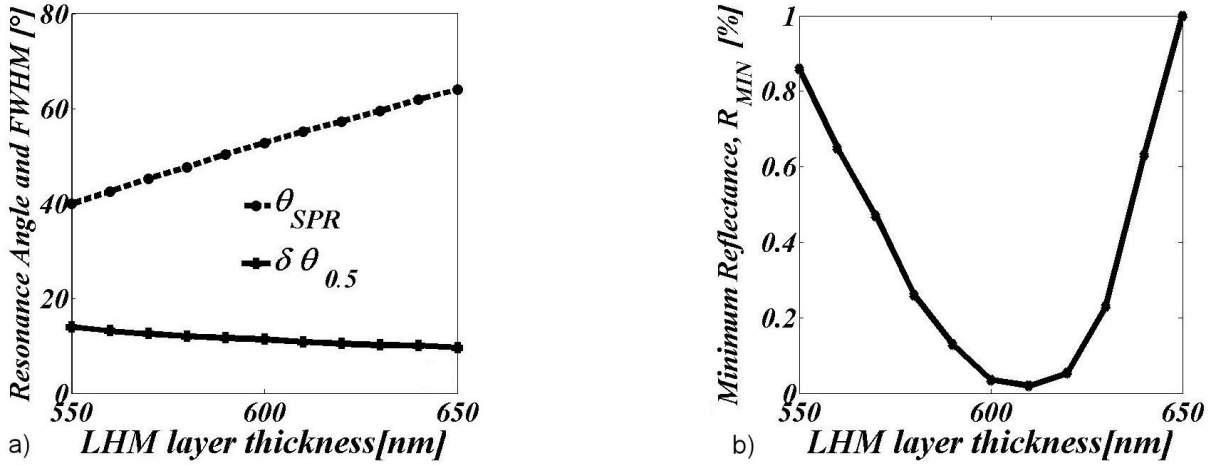

FIGURE 8. a) Variation of resonance angle and FWHM of SPR sensor and b) Variation of minimum reflectance, with thickness of LHM layer between 550 nm and 650 nm.

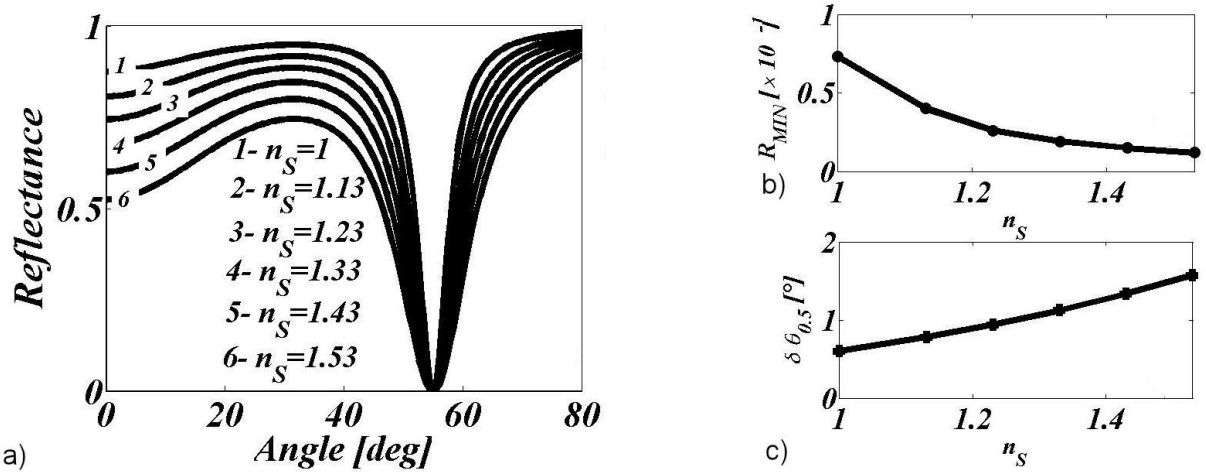

FIGURE 9. a) Reflectance as function of the incidence angle, b) the minimum reflection and c) FWHM the SPR angle under the change indices refractive of sensing medium with the LHM thickness of 610 nm; the other parameters are the same in Fig. 6.

with the appropriate thicknesses of all the structure's layers [16]. In the Fig. 8, The acceptable conditions in terms of minimum dip depth, and reduced FWHM are achieved for 610 nm -LHM thickness. Based on the previous data, analytical dependencies between the intrinsic characteristics retrieved from p-reflectivity curves versus influence thickness of LHM layer between 550 nm and 650 nm. can be derived as follows:

(i) Dip depth of p-reflectivity versus LHM layer thickness

$$R[\%] = 3.06\times10^{(-6)}d^3 - 0.0052d^2 - 21327d - 532.7. \quad (16)$$

(ii) FWHM versus LHM layer thickness

$$\triangle\,\theta_{0.5}[^\circ] = 0.041d + 36.28 \pm 0.76. \quad (17)$$

(iii) Resonance condition versus LHM layer thickness

$$\theta_{SPR}[^\circ] = 0.24d - 92 \pm 0.92. \quad (18)$$

3.2. Influence of sensing medium refractive index

For a complementary analysis, it is important to evaluate the effect on p-reflectance behaviors with RI change of the sensing medium, ns. Results shown in Fig. 9a), predict that the increase of sensing medium RI from 1 to 1.55 increases the FWHM and increases the coupling strength between light and incident photons near LHM layer-sensing medium interface. Here, SP resonance condition remains insensitive to the sensing medium RI change, but the coupling strength is. Figures 9b) and 9c), indicate the evolution of dip depth and FWHM correlated to the SP mode versus sensing medium RI, with their analytical forms written:

(i) Dip depth of p-reflectivity versus sensing medium RI

$$R[\%] = 29.7n_S^2 - 81.6n_S + 16 \pm 0.049. \quad (19)$$

(ii) FWHM versus sensing medium RI

$$\triangle\,\theta_{0.5}[^\circ] = 1.2n_S^2 - 1.24n_S + 0.63 \pm 0.0074. \quad (20)$$

Finally, the intrinsic angular sensitivity defined as the ration between the shift of resonance angle and RI change ($S_\theta = \triangle\theta_{SPR}/\triangle\, n_S$) gets zero value, and it can be possible to include the evaluation of sensitivity in terms of minimum p-reflectance, $S_R = \triangle R_{SPR}/\triangle\, n_S$ that is evaluate as:

$$S_R = 0.594n_S - 0.816. \quad (21)$$

3.3. SPR change from prism-LHM layer-ambient air

In this subsection, we consider ambient air as an outer medium, and LHM layer thickness is adjusted from 610 nm to 810 nm. For this proposed sensor, p-reflectance curves displayed in Fig. 10, reveal a significant effect include on the change of LHM layer thickness. In other hand, the proposed sensor exhibits an SP resonance located in the angular range of $50 - 60^\circ$ and other SP peak can be coexisted at lower incident angle. According to this observations, it is important to turn LHM layer thickness in the wavelength regime, $d > \lambda$. Such conditions are described from p-reflectance plots reported in Figs. 11-13.

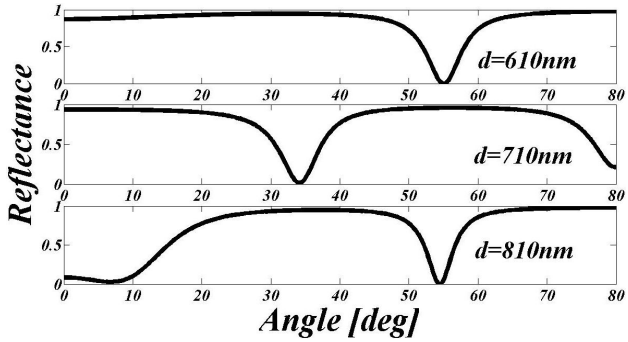

FIGURE 10. Dependencies of SPR spectrum in 2S2G-LHM layer-ambient air, for different LHM thicknesses 610 nm, 710 nm and 810 nm. The other parameters are the same in Fig. 6.

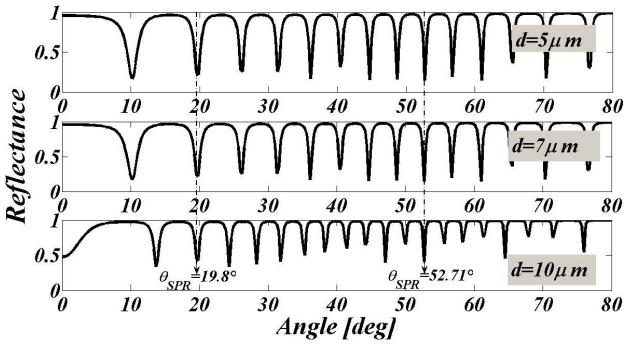

FIGURE 11. Evolution of the SPR micro structured with refractive indices of sensing medium: $ns = 1$ and different LHM thickness of 5 μm, 7 μm and 1 μm; the other parameters are the same in Fig. 6.

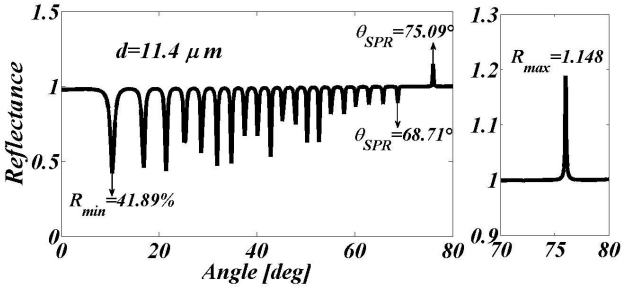

FIGURE 12. The reflection spectrum in micro structured with refractive indices of sensing medium: $n_S = 1$ LHM thickness of 11.4 μm; the other parameters are the same in Fig. 6.

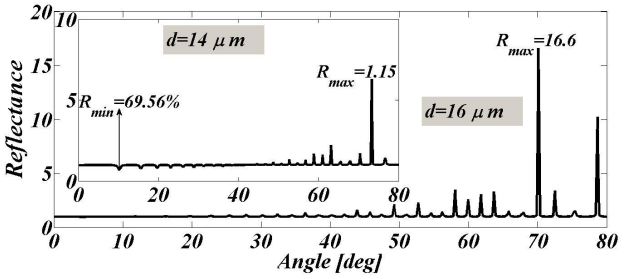

FIGURE 13. The reflection spectra from 2S2G glass-LHM layer-ambient air with LHM layer thickness adjusted from 14 μm to 16 μm.

According to these results, LHM layer thickness gives the ability to generate multiple SPs oscillations as angular periodicity between two successive peaks can be controlled. Beyond 7 μm-LHM layer thickness, angular periodicity decreases and positives peaks with dominant intensity appear. The presence of multiple SPs oscillations is mainly to the production of multiple reflection of light inside the LHM, and it remains to explain the dominant intensity induced on adjusting LHM layer thickness beyond 11.4 μm.

4. Conclusions

In this analytical study, we have investigated the limit of a proposed SP sensor in terms of reducing the FWHM peak displayed on angular p-reflectance plot. It is observed that LHM layer thickness adjusted in wavelength regime leads to predict the functionality of Fabry-Perot interferometer. In the subwavelength scale, the proposed sensor exhibits an SP peak with moderate characteristics that can be considered in the field of optical sensing technology.

Acknowledgements

The authors gratefully acknowledge useful discussions conducted by all the members of the supervisor Professor Benamar BOUHAFS, on the subject of the Plasmonics Nanostructures and their Applications.

1. E. Kretschmann and H. Raether, Radiative decay of non-radiative surface plasmons excited by light, *Z. Naturforsch. A* (1968) 2135.

2. A. Cherifi, and B. Bouhafs, Potential of SPR sensors based on multilayer interfaces with gold and LHM for biosensing applications, *Photonic Sensors* **7** (2017) 199.

3. S.A. Taya, and HM. Kullab, Optimization of transverse electric peak type metal clad waveguide sensor using double negative materials, *Appl. Phys. A* **116** (2014) 1841.

4. F. Xiao, G. Li, K. Alameh, and A. Xu, Fabry-Pérot-based surface plasmon resonance sensors, *OPTICS LETTERS* **37** 201

5. M. Walser, Electromagnetic metamaterials , Proc. SPIE-Complex mediums I I, *Beyond linear isotropic dielectrics*, **4467** (2001) 1, https://doi.org/10.1117/12.432921.

6. C. Bourel, Thesis from the Université du sud Toulon-Var, (2010).

7. R. A. Shelby, D.R. Smith, S. Schultz, Experimental verification of a negative index of refraction, *Science* **292** (2001) 77.

8. L. Zhou, and C. Chan, Vortex-like surface wave and itsrole on the transient phenomena of metamaterial focusing, *Appl. Phys. Lett.* **86** (2005) 101104.

9. V. G. Veselago, The electrodynamics of substances with simultaneously negative values of permittivity and permeability, *Sov. Phys. Usp*. **10** (1968) 509.

10. Y. Liu and X. Zhang, *Chem. Soc. Rev*, **40** (2011) 2494.

11. S. M. Xiao, and al, Loss-free and active opticalnegative index metamaterials, *Nature* **466** (2010) 735-738.

12. K.Park, B. J. Lee, C. Fu, W.M. Zhang, Study of the surface and bulk polaritons whith a negative index metamaterial, *J. of the optical society of America, B* **22** (2005) 1016.

13. L. Novotn y and B.Hechet, *Principles of Nano-Optics*, (Cambridge University, New York, 1990).

14. S. Pal, Y.K. Prajapati, J.P. Saini, V. Singh, Sensitivity enhancement of Meta-material-based surface plasmon resonance biosensor for near infrared, *Optica Applicata*, **XLVI** (2016) 131-143.

15. R. Jha and A K. Sharma, Chalcogenide glass prism based SPR sensor with Ag?Au bimetallic nanoparticule alloy in infrared wavelength region, *J. Opt. A: Pure Appl. Opt*, **11** (2009) 04550.

16. B.A. Snopok *et al.*, Optical biosensors based on the surface plasmon resonance phenomenon: Optimization of the metal layer parameters, Semi-conductor physics, *Quantum Electronics and Optoelectronics* **4** (2001) 65-69.